PHYSICAL REVIEW A VOLUME 11, NUMBER 6 JUNE 1975

Hartree-Slater calculation of the cross section for L-shell ionization of argon by simple heavy charged particles*

Byung-Ho Choi†
University of North Carolina at Chapel Hill, Chapel Hill, North Carolina 27514
(Received 12 December 1974)

The cross sections for L-shell and subshell ionization by direct Coulomb excitation of argon by incident heavy charged particles are evaluated. Incident particles are described in the plane-wave Born approximation, and nonrelativistic Hartree-Slater (HS) wave functions are used for the atomic electrons. Form factors, energy distributions, and ionization cross sections are compared with those obtained from screened hydrogenic wave functions. At most incident energies the HS results for the total ionization cross section are only slightly smaller than those obtained with screened hydrogenic wave functions, but considerable discrepancies are found for form factors and energy distributions near the ionization threshold.

I. INTRODUCTION

The ionization cross sections of inner atomic shells by incident heavy charged particles such as protons or α particles are being measured with ever improving accuracy.[1] In particular, attention has recently turned to the high-resolution determination of the characteristic x rays produced following the creation of vacancies in inner atomic shells. To interpret the experimental data, calculations of the ionization cross section for K, L, and M shells and their subshells have been made based on the plane-wave Born approximation (PWBA).[2-6] In this approximation, incident and inelastically scattered particles are described by plane waves, while screened hydrogenic (SCH) wave functions have been used for the atomic electrons. For sufficiently high incident projectile energies such that the direct Coulomb excitation process is dominant in inner-shell ionization, the PWBA seems to be adequate. Furthermore, the use of SCH wave functions for K-shell ionization is entirely appropriate. However, for the ionization of L electrons, where the screening effects of outer electrons are important, the SCH wave functions are not expected to be realistic, particularly, for the electrons ejected with low kinetic energies, even though the orthogonality conditions between the initial and final wave functions are satisfied. Therefore, it is desirable to perform calculations on the inner-shell ionization process using more realistic wave functions.

Recently, some authors[7,8] have made calculations on the ionization of electrons by heavy charged particles employing nonrelativistic Hartree-Slater (HS) atomic wave functions.[9] However, these authors either evaluated total ionization cross sections for very light elements or some differential energy transfer cross section for L electrons in certain elements at a few selected incident energies.

In this paper, total L-shell and subshell Coulomb ionization cross sections have been evaluated for argon as a function of the incident energies, using again nonrelativistic HS wave functions for the atomic electrons. In addition to providing theoretically calculated L-shell vacancy production cross sections for argon targets, these calculations are intended to test how much the total ionization cross section is affected by the use of a realistic wave function in comparison with SCH wave functions as the incident energy is varied. The use of a relativistic HS wave function would not appreciably alter these results.

The method is briefly outlined in Secs. II and III, including numerical procedures of computation. Results of the present calculations on the L-shell and subshell ionization cross sections for argon are presented in Sec. IV and compared with calculations using SCH wave functions, and a discussion of the results is given.

II. L-SHELL IONIZATION CROSS SECTION

In the nonrelativistic PWBA, the ionization cross section for electrons ejected from the L-subshell by an incident heavy charged particle is given by[2]

$$\sigma_{L_s} = \int_{W_{\min}}^{\infty} dW_{L_s} \frac{d\sigma_{L_s}}{dW_{L_s}} \quad (L_s = 2s, 2p). \tag{1}$$

The energy transfer cross section, $d\sigma_{L_s}/dW_{L_s}$, is expressed as

$$\frac{d\sigma_{L_s}}{dW_{L_s}} = \frac{8\pi Z_1^2 a_0^2}{Z_2^4 \eta} \int_{Q_{\min}}^{Q_{\max}} \frac{dQ}{Q^2} \left| F_{W_{L_s}, L_s}(Q) \right|^2, \tag{2}$$

$$\eta = \frac{mE}{MZ_2^2 R_\infty}, \quad W_{L_s} = \frac{\Delta E}{Z_2^2 R_\infty}, \quad Q = \frac{q^2 a_0^2}{Z_2^2}. \tag{2'}$$

Here, M and E are the mass and energy of the incident particle, ΔE and $\hbar\vec{q}$ are the energy and momentum transfers of the incident particle to the L_s electron, m is the mass of the electron.[10] $Q_{\min}$ and $Q_{\max}$ are established from energy and momentum conservation, and it is sufficiently accurate to set $Q_{\min} = W_{L_s}^2/4\eta$ and $Q_{\max} = \infty$. For the lower limits, $W_{\min}$, of the energy transfer, we introduce the HS binding energies of $2s$ and $2p$ electrons (311 and 248 eV for $2s$ and $2p$ electrons of argon, respectively).[9] The square of the form factor, $|F_{W,nl_i}(Q)|^2$, for the transition between electronic states,

$$|F_{W,nl_i}(Q)|^2 = \sum_{m_i l_f m_f} \left| \int e^{i\vec{q}\cdot\vec{r}} \Psi^*_{kl_f m_f}(\vec{r}) \Psi_{nl_i m_i}(\vec{r})\, d\vec{r} \right|^2$$

$$= (2l_i+1) \sum_{l l_f} (2l+1) \langle l_i l 00 \mid l_f 0\rangle^2 \left| \int j_l(qr) R_{kl_f}(r) R_{nl_i}(r)\, dr \right|^2 , \tag{3}$$

where

$$\Psi_{kl_f m_f}(\vec{r}) = \frac{R_{kl_f}(r)}{r} Y_{l_f m_f}(\theta, \phi)$$

is the real continuum partial wave of ejected electrons normalized per unit energy interval in units of $Z_2^2 R_\infty$.

The bound and continuum radial wave functions, $R_{nl_i}(r)$ and $R_{kl_f}(r)$, are the solutions of the Schrödinger equation with the central HS potential $V(r)$. In the atomic unit system where $e^2 = \hbar^2 = 2$ and $m = 1$ (i.e., electronic energies in units of R_∞, and r in units of a_0), which we shall use hereafter unless specified otherwise, the radial equation is

$$\left(-\frac{d^2}{dr^2} + V(r) + \frac{l(l+1)}{r^2} - E \right) R(r) = 0 , \tag{4}$$

with

$R(r) = R_{nl_i}(r)$ or $R_{kl_f}(r)$,

$l = l_i$ or l_f,

and

$E = E_{nl}$ or k^2.

Here, $-E_{nl}$ is the binding energy of nl-subshell electrons, and $V(r)$ is of the form

$$V(r) \to -2Z_2/r \text{ as } r \to 0$$

and

$$V(r) = -2/r \quad \text{for } r \geq r_c . \tag{5}$$

The meaning of cutoff radius r_c, introduced by Latter,[11] is described in Ref. 9.

III. NUMERICAL PROCEDURES AND ACCURACY

The HS potential $V(r)$ and the bound-state wave functions $R_{2s,p}(r)$ are generated using the program in Herman-Skillman,[9] and the continuum wave function $R_{kl_f}(r)$ is obtained by integrating the radial Schrödinger equation [Eq. (4)] with Numerov's method. Integration step sizes were the same as those used in Ref. 9 through the first 121 mesh points. Beyond this point where Herman-Skillman integration step sizes do not give accurate results for large kinetic energies and rapidly oscillating wave functions, a constant step size was used. Normalization factors of continuum wave function were determined by noting that

$$U_l(r) = AF_l(r) + BG_l(r) \quad \text{for } r \geq r_c$$

with (6)

$$A = N' \cos\delta_l, \quad B = N' \sin\delta_l$$

where $U_l(r)$ is an unnormalized radial solution of Eq. (4), and $F_l(r)$ and $G_l(r)$ are the regular and irregular Coulomb wave functions with the parameter which behave as sine and cosine function in the asymptotic region. N' and δ_l are obtained by satisfying Eq. (6) at two points $r_1, r_2 \geq r_c$. Thus,

$$R_{kl}(r) = NU_l(r)$$

with

$$N = Z_2 \left(\frac{1}{\pi k(1+\alpha^2)} \right)^{1/2} \frac{F_l(r_1) + \alpha G_l(r_1)}{U_l(r_1)} ,$$

$$\alpha = \tan\delta_l = \frac{U_l(r_2)F_l(r_1) - U_l(r_1)F_l(r_2)}{U_l(r_1)G_l(r_2) - U_l(r_2)G_l(r_1)} . \tag{7}$$

Numerical methods for computing $F_l(r)$ and $G_l(r)$ are given in literature.[12] The two matching points, r_1 and r_2, were chosen 20–30 step sizes apart, although the numerical accuracy is not sensitive to the choice of r_1 and r_2. For computing $j_l(qr)$, recurrence relations of decreasing or increasing

order of l were used, depending on whether $qr < l_{max}$ or $qr \geq l_{max}$, where l_{max} ($\simeq 20$) is the largest l value considered here. The step sizes for the radial integration to obtain the form factors generally depend on Q; in order to achieve accurate results, for high Q values they should be similar to those used in integrating the Schrödinger equation. The Newton-Cotes method was employed for the radial overlap integration up to $r \simeq 4.5$.

To check the numerical accuracy, we have evaluated hydrogenic form factors for several values of Q and W for argon employing the same numerical procedures. The numerically evaluated form factors agreed with analytically obtained hydrogenic form factors[4] to within 0.1%.

IV. RESULTS AND DISCUSSIONS

Total Coulomb ionization cross sections of $2s$, $2p$ electrons of argon ($Z_2 = 18$) were evaluated for several incident energies of up to 20 MeV/amu. The integration over the energy transfer W in Eq. (1) was terminated at around $W = 1.35$, and this was sufficient to compute the total ionization cross section to within 0.1% accuracy. The partial-wave contributions depend on the incident energy and the energy transfer. However, in general, the number of partial waves required to obtain the desired accuracy increases as the energy transfer increases, and this requires a considerable amount of computer time for large energy transfer. Near the ionizing threshold, a few partial waves (l, $l_f = 3 \sim 4$) were taken, while about 20 partial waves are needed around $W = 1.35$ in the present calculations.

To understand the behavior of the cross sections, we present first the square of the form factors for HS and SCH in Figs. 1 and 2 for $2s$ and $2p$ electrons, respectively. The SCH form factors are obtained from the analytic expressions with an effective nuclear charge $Z_L = 18 - 4.15 = 13.85$ for the L shell of argon. The SCH results were in Ref. 4, multiplied by $(Z_2/Z_L)^2$ to get the same continuum-wave-function normalization as in the present calculation. Similar conversions were made for Q and W, since in the hydrogenic calculations these were defined in terms of Z_L rather than the full nuclear charge Z_2.

It is interesting to note that both HS and SCH form factors for $2s$ electrons show secondary maxima in the large-Q region, arising from a node in the bound-state radial wave function. Discrepancies between the HS and SCH form factors are considerable near the ionizing threshold, where SCH form factors are much larger than those for HS, particularly for small values of Q. In addition, the SCH form factors are bigger than HS form factors near the peak of the secondary maxima for the $2s$ electron ionization. At sufficiently large energy transfer, the two calculations agree closely for all Q except the largest values. In Fig. 3, comparisons are shown between the HS and SCH calculations of the products of radial wave functions, $R_{2s,p}(r) \times R_{kl}(r)$, which occur in the expression of form factors [Eq. (3)] for the optically allowed $2p$-s wave and $2s$-p wave transitions, which are dominant in the low-momentum-transfer region. Near the nucleus, the HS potential $V(r)$ is deeper (more attractive) than the SCH potential, $-2Z_L/r + C$, where $C = Z_L^2/4 - I_0$, and I_0 may be either the experimental or the HS binding energy of $2s$, $2p$ electrons. For an intermediate region of r, the HS potential becomes less attractive than that of SCH, while for sufficiently large r, it is again always more attractive than the SCH potential. This can be seen in terms of the wave functions in Fig. 3. The difference between the two potentials significantly affects the continuum wave functions near the ionizing threshold, and the discrepancy between

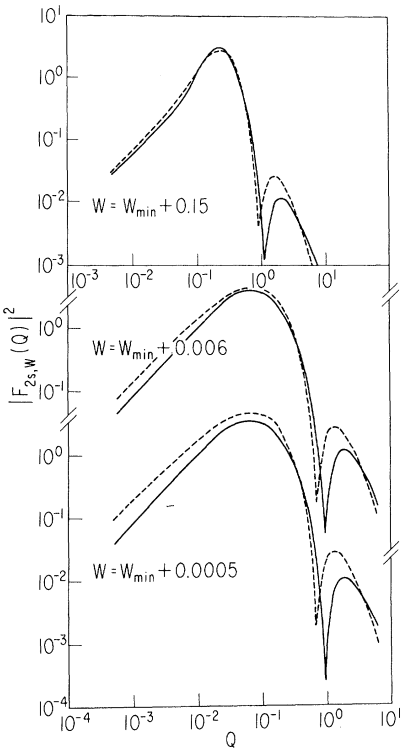

FIG. 1. $2s$-subshell form factors, $|F_{2s,W}(Q)|^2$, of Ar as functions of momentum transfer Q for sample energy transfers $W = W_{min} + 0.0005$, 0.006, 0.15. Solid lines denote the form factors with HS wave functions of the present calculation, and dashed lines are those with SCH wave functions. W_{min} is the HS binding energy of $2s$ electrons.

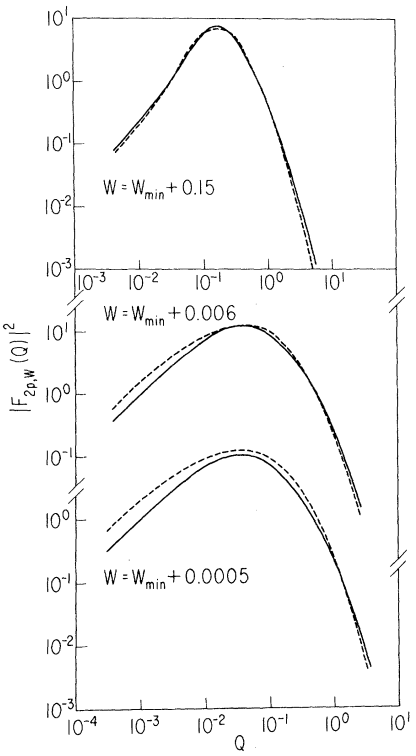

FIG. 2. Same as Fig. 1 for the $2p$ subshell. See the explanations of Fig. 1 for corresponding quantities.

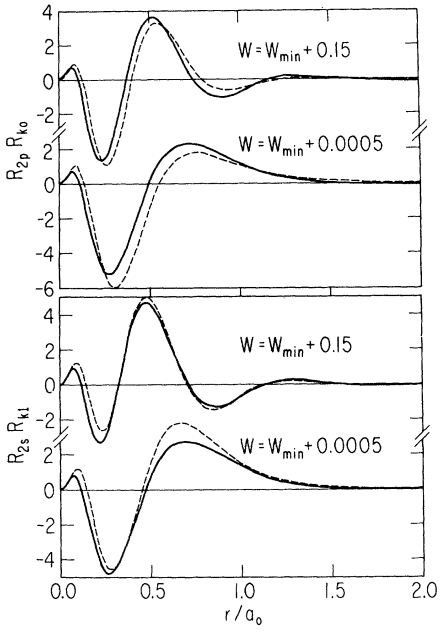

FIG. 3. Overlaps between initial and final radial wave functions, $R_{2s,p}(r)R_{kl}(r)$, at energy transfers $W = W_{\min} + 0.0005$, 0.15. Only $2s$-p wave and $2p$-s wave transitions are shown. Solid lines are those obtained from HS potential, and dashed lines are SCH results.

two form factors for small Q can be understood from the figure. It should be remembered that the SCH continuum wave functions are not realistic near the ionizing threshold in the sense that, in general, they diverge as r goes to infinity, although the products with the bound-state wave functions decrease exponentially.

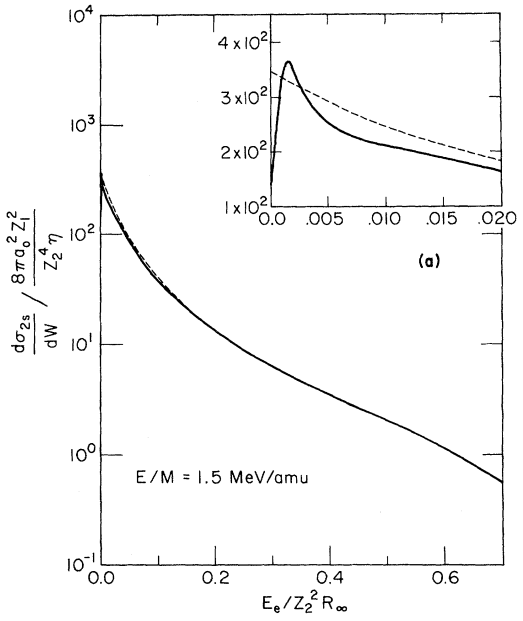

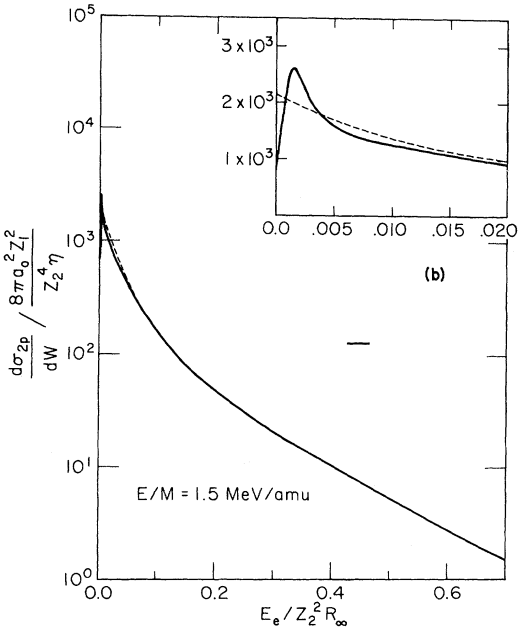

FIG. 4. Energy distributions, $(d\sigma_{2s,p}/dW)/(8\pi a_0^2 Z_1^2/Z_2^4\eta)$, as functions of electronic energy, $E_e/Z_2^2 R_\infty$, for incident energy $E/M = 1.5$ MeV/amu and for (a) $2s$ electrons and (b) $2p$ electrons. Solid lines are those obtained from HS potential, and dashed lines are SCH results.

TABLE I. L-subshell ionization cross sections $\sigma_{2s,p}/Z_1^2$ for argon with HS wave functions, compared with those with SCH wave functions.

E/M (MeV/amu)	HS	SCH (HS binding energy)	SCH (Experimental binding energy)
		σ_{2s}/Z_1^2 (10^{-19} cm^2)	
0.12	2.4679	2.6377	2.3839
0.3	6.2595	6.4750	6.0955
0.7	7.2791	7.5001	7.1594
1.5	5.5351	5.8847	5.6341
3.0	3.5764	3.9363	3.7660
8.0	1.6826	1.9440	1.8556
20.0	0.7922	0.9463	0.9017
		σ_{2p}/Z_1^2 (10^{-19} cm^2)	
0.12	13.227	13.801	14.066
0.3	26.266	26.352	26.720
0.7	31.628	31.690	32.056
1.5	26.876	27.765	28.074
3.0	19.064	20.321	20.559
8.0	9.8293	10.891	11.035
20.0	4.8862	5.5745	5.655

Sample energy distributions of $2s, 2p$ electrons with HS wave functions are presented in Fig. 4 and compared with those for SCH, corresponding to an incident velocity given by $E/M = 1.5$ MeV/amu. For purposes of comparison, the same HS binding energies are used in both calculations. The energy distributions for HS and SCH differ only in the small-energy-transfer region near the ionizing threshold and essentially coincide elsewhere, as expected from the behavior of the form factors. This indicates that the difference between two potentials is negligible compared with the kinetic energies of the electrons when the energy transfer $W \gtrsim 0.5$. In the HS calculations, at very low energy transfer, around $0.0015 Z_2^2 R_\infty$ kinetic energy of the ejected electrons, a maximum occurs in the energy distribution. This "delay" of the monotonic decrease of the electron energy near the ionizing threshold has been noted earlier by some authors.[8,13] It should be noted that at the maximum the HS differential cross section is greater than the SCH result for this incident energy. As the incident energy increases, the discrepancy between the two calculations will be more significant near threshold.

Sample values of total ionization cross sections of $2s, 2p$ electrons of argon calculated with HS wave functions, are presented in tabular form in Table I for several incident energies up to 20 MeV/amu and compared with the corresponding SCH results obtained from Ref. 4. The results are also displayed in Figs. 5 and 6 for $2s$ and $2p$ electrons, respectively. As noted earlier, $W_{\min}$ was taken to be the HS binding energy of $2s$ and $2p$ electrons in both calculations. However, since experimental binding energies have been used for SCH calculations in the interpretation of experimental data, we also present the corresponding results in the table and figures. (The experimental binding energies of L_1-, L_2-, and L_3-subshell electrons are 320.0, 247.3, and 245.2 eV, respectively.)

In spite of the fact that the electron energy distributions show significant discrepancies near the ionizing threshold, the integrated total cross sections do not show much difference between the two

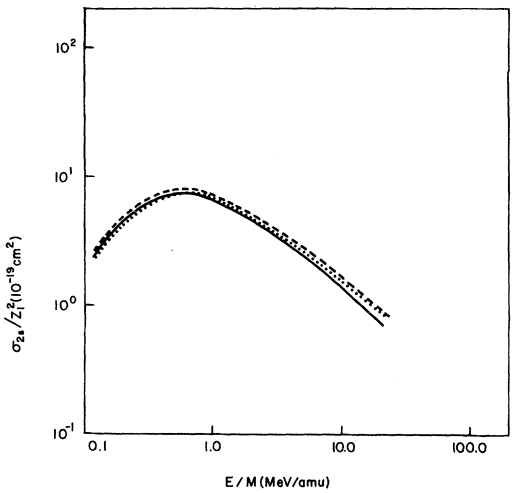

FIG. 5. $2s$-subshell ionization cross section, σ_{2s}/Z_1^2, as functions of incident energy E/M. The solid line is the present result of HS calculation. Dashed and dotted lines are the SCH results with HS and experimental binding energies of $2s$ electrons, respectively.

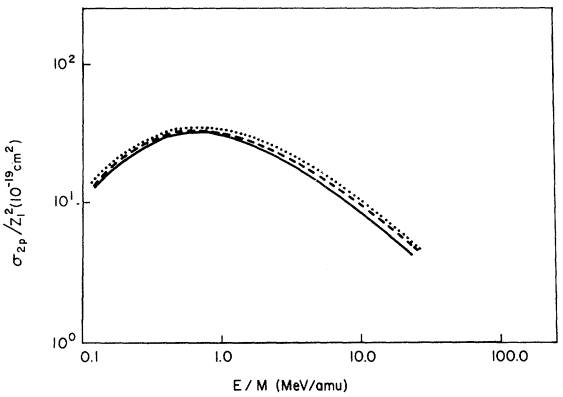

FIG. 6. Same as Fig. 5 for $2p$ subshell. See the explanation of Fig. 5 for corresponding quantities.

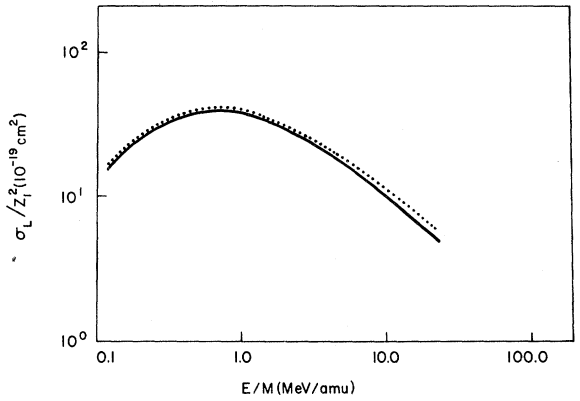

FIG. 7. Total L-shell ionization cross section, σ_L/Z_1^2, as functions of incident energy E/M. Solid line is the present work of HS calculation and dotted line is that of SCH with experimental binding energies of L-subshell electrons.

calculations. In general, the HS cross sections are slightly smaller than those of SCH, if one employs the same binding energies. However, the experimental binding energy for $2s$ electrons (320 eV) is considerably bigger than that of HS (311 eV), and the SCH ionization cross sections for $2s$ electrons computed with the experimental binding energy are slightly smaller than those of HS in the intermediate low incident energy region. In the very low incident energy region, where Q_{min} is near the secondary maximum of the form factor for $2s$ electrons, the SCH cross section will be much bigger than that of HS, as can be seen from Fig. 1 and Eq. (2), and both cross sections will show sharp kinks.[14] However, measurements of K-shell ionization cross sections for light elements ($Z_2 = 13 \sim 20$) show that the PWBA predictions with SCH wave functions overestimate the experimental data by factors of 4 to 5 in this low incident energy region.[15] This suggests that also for L-shell ionization, the plane-wave description for incident particles may not be adequate and that improvements of the projectile wave functions may be more important for this energy region. Therefore, we are presenting results here only for an incident energy region where the PWBA is reasonably valid.

As the incident energy increases, the HS cross sections are seen to become smaller than SCH cross sections. This can again be understood from the behavior of form factors in the small-Q region [cf. Figs. 1, 2, and Eq. (2)]. The total L-shell ionization cross section for argon is shown in Fig. 7 again based on SCH and HS calculations. It seems doubtful that the differences are sufficient to be detectable by experiment. Much larger discrepancies between the two calculations may be found for lighter elements than argon, such as neon, carbon, and aluminum. Experimental data on the L-shell ionization cross sections for light elements, say, $Z_2 = 10 \sim 20$, are needed to test improved atomic wave functions.

ACKNOWLEDGMENTS

The author wishes to express a deepest appreciation to Professor Eugen Merzbacher for many valuable discussions and suggestions. The author is also grateful to Dr. D. H. Madison for discussions of integration step sizes and numerical accuracy.

*Work supported by the U. S. Atomic Energy Commission.

†Now at Theoretical Chemistry Institute, University of Wisconsin, Madison, Wisc. 53706.

[1]For recent experimental data on the inner-shell ionization cross sections, see *Proceedings of the International Conference on Inner-Shell Ionization Phenomena and Future Applications, Atlanta, Georgia, 1972*, edited by R. W. Fink, S. T. Manson, J. M. Palms, and P.V. Rao, CONF-720 404 (U. S. Atomic Energy Commission, Oak Ridge, Tenn., 1973).

[2]E. Merzbacher and H. W. Lewis, *Handbuch der Physik*, edited by S. Flügge (Springer-Verlag, Berlin, 1958), Vol. 34, p. 166.

[3]G. S. Khandelwal, B.-H. Choi, and E. Merzbacher, At. Data 1, 103 (1969).

[4]B.-H. Choi, E. Merzbacher, and G. S. Khandelwal, At. Data 5, 291 (1973).

[5]B.-H. Choi, Phys. Rev. A 7, 2056 (1973).

[6]D. H. Madison and E. Merzbacher, in *Atomic Inner-Shell Processes*, edited by B. Crasemann (Academic, New York, to be published).

[7]E. J. McGuire, Phys. Rev. A 3, 267 (1971).

[8]S. T. Manson, Phys. Rev. A 6, 1013 (1972).
[9]F. Herman and S. Skillman, *Atomic Structure Calculations* (Prentice-Hall, Englewood Cliffs, N. J., 1963).
[10]For notations, see Refs. 3 and 4.
[11]R. Latter, Phys. Rev. 99, 510 (1955).
[12]B. Buck, R. N. Maddison, and P. E. Hodgson, Phil. Mag. 5, 1181 (1960).
[13]For experimental situation with electron impact, cf. V. V. Afrosimov, Yu. S. Gordeev, V. M. Lavrov, and S. G. Shchemelinin, Zh. Eksp. Teor. Fiz. 55, 1569 (1968) [Sov. Phys.—JETP 28, 821 (1969)].
[14]These are shown for σ_{2s} with SCH wave functions by E. Merzbacher in Ref. 1, and for σ_{3s} with the same wave functions in Ref. 5.
[15]Cf., e.g., W. Brandt, in Ref. 1.